The ^{96}Mo$(\vec{p},d)^{95}$Mo reaction at 50 MeV

S. A. Sultana,* D. Maki, G. Wakabayashi, Y. Uozumi, and N. Ikeda
Department of Applied Quantum Physics and Nuclear Engineering, Kyushu University, Fukuoka 812-8581, Japan

Syafarudin
P2TKN-BATAN, Kawasan PUSPIPTEK Serpong, Indonesia

F. Aramaki
Kyushu Institute of Information Sciences, Dazaifu 818-0117, Japan

T. Kawaguchi and M. Matoba
Faculty of Engineering, Kyushu Sangyo University, Fukuoka 813–8503, Japan

H. M. Sen Gupta
Department of Physics, University of Dhaka, Dhaka, Bangladesh
(Received 22 March 2004; published 30 September 2004)

The ^{96}Mo$(p,d)^{95}$Mo reaction has been studied with a 50 MeV polarized beam. Differential cross sections and analyzing powers have been measured for investigating the level structure in ^{95}Mo up to the excitation energy of 5.8 MeV. The standard distorted-wave Born approximation theory provides transfer angular momentum values and spectroscopic factors for the excited states. Furthermore, the theoretical analysis is extended also for the continuum region with a direct reaction model. Experimental double differential cross sections for continuum spectra are predicted well by adopting an asymmetric Lorentzian form for the response function in the distorted wave Born approximation based cross section calculations.

DOI: 10.1103/PhysRevC.70.034612 PACS number(s): 21.10.Hw, 21.10.Jx, 21.10.Pc, 24.10.Eq

I. INTRODUCTION

There has been a large number of investigations on the single-neutron pickup reactions on nuclei covering the entire periodic table and these have been proved useful in providing information on the neutron hole structure in nuclei. Although many investigations have been done for analyzing the level structure in a nucleus, almost all the works have been performed with unpolarized incident beams. These studies were mostly concerned only with the discrete levels and no information is available on the continuum spectra which appear just above the discrete excitation levels. Theoretical models have been proposed to study the continuum spectra for one nucleon transfer reaction [1–3], which cannot reproduce well the experimental data [4,5] and also there are no discussions on the ensemble of discrete levels.

The present work is concerned with the (p,d) reaction on ^{96}Mo using a polarized beam at 50 MeV.

Differential cross sections and analyzing powers for the ^{96}Mo$(p,d)^{95}$Mo reaction are measured with 50 MeV polarized protons for discrete levels, and the results are analyzed to assign spin-parities and determine spectroscopic factors of excited neutron-hole states in the excitation region of 0–4.95 MeV. The experimental data are analyzed by the standard distorted wave Born approximation (DWBA) calculations.

For the theoretical investigation of double differential energy spectra of cross section, an approach proposed by Lewis [6] was employed here, which is based on the DWBA and an asymmetry Lorentzian form strength function.

The present work was undertaken in view of the fact that the spin-parities of almost all the levels in ^{95}Mo above $Ex \sim 1.1$ MeV or so are uncertain [7]. Also, neutron pickup reactions on ^{96}Mo were carried out previously using (p,d) [8], (d,t) [8–11], and $(^3He,\alpha)$ [12] reactions with unpolarized beams. The use of a polarized beam, as in the present work, allows one to assign the (ℓ,j) transfer with much less ambiguities to levels from the simultaneous analyses of the differential cross section and analyzing power. Further to the discrete levels studied in the neutron pickup reactions as earlier [8–12] continuum spectra were also investigated in this present study. However, in this study spectrum regions from discrete levels to continuum were treated with a global analysis using the direct reaction model and continuous strength functions based on DWBA cross sections. The optical model potentials in both the entrance and exit channels are also better defined in a (p,d) reaction than the triton, ^3He and alpha particles in the (d,t) and $(^3He,\alpha)$ reactions, specially if an adiabatic potential is employed for deuterons [13]. This is done in our study. The spectroscopic factors are therefore expected to be more reliable for levels with a good fit simultaneously to both angular distribution and analyzing power in a $(\vec{p},d)$ reaction than in the other neutron pickup reactions. Similar studies have been carried out by some of the present authors on two other Mo isotopes using polarized proton beams, namely ^{92}Mo at 65 MeV and ^{100}Mo at 21 and 50 MeV [14–16] and also on several nuclei covering the wide mass range from ^{40}Ca to ^{208}Pb [14–22]. The present

*Electronic address: sadia_afroze@yahoo.com

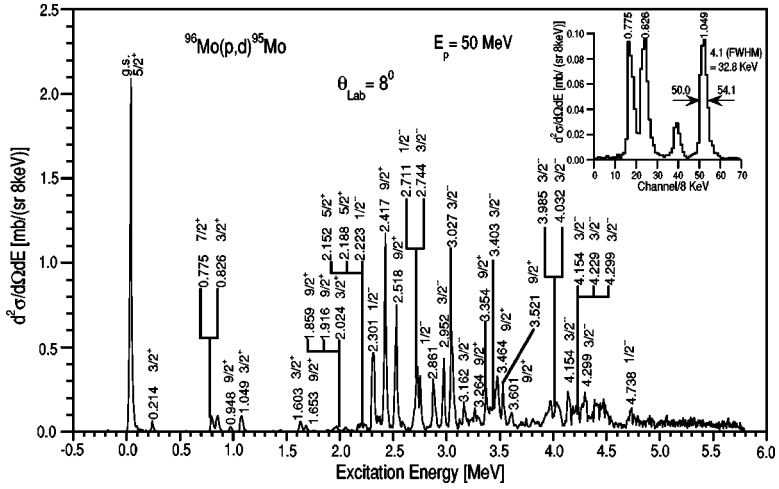

FIG. 1. Typical energy spectrum of deuterons from the ^{96}Mo$(\vec{p},d)^{95}$Mo reaction at 50 MeV.

work is a follow up of these studies as performed on another Mo isotope, namely ^{96}Mo and the results obtained are compared with previous neutron pickup studies on ^{96}Mo, all of which are with unpolarized beams, as well as with ^{92,100}Mo$,(\vec{p},d)$ reactions.

II. EXPERIMENT

A. Experimental procedure

The experiment was carried out with a beam of polarized protons of energy 50 MeV obtained from the AVF cyclotron of the Research center for Nuclear Physics (RCNP), Osaka University. We took here polarized proton beam as a incident particle from the consideration that $(\vec{p},d)$ reaction provides more exact procedure in deducing the spectroscopic factor value and our cyclotron facility is optimized to accelerate polarized protons and also the experimental system has better conditions in target energy losses and particle identification compared with use of (d,t) reactions. Incident energy at 50 MeV was taken from the interest first for experimental facilities availability because the AVF cyclotron of the RCNP, Osaka University, can accelerate a polarized proton beam well in several tens of mega-electron-volt energy region and second as a part of our detailed research on Mo isotopes, discussed in Sec. I.

The target was self-supporting, isotopically enriched ($\sim$98% of ^{96}Mo) and of thickness 0.79 mg/cm^2. The emitted deuterons were momentum analyzed using the RAIDEN [23] viewed with the focal plane detector system KYUSHU [24]. The angular distributions of cross sections and analyzing powers were measured over the laboratory angles 8°–48°. The measured energy range corresponds to the excitation energy region up to about 5.8 MeV. The higher excitation region had a considerable "contamination" arising from the protons elastically scattered. The data were therefore not considered to be reliable to study. No such contaminant was found in the region of ground state to E_x=5.8 MeV or so. The normalization of the absolute cross section was performed by scaling the measured $p+^{96}$Mo elastic scattering cross section to the optical model prediction at small angles using the global potential of Menet *et al.* [25]. The spurious data due to impurities were removed from the experimental spectra by fitting a Gaussian function to each peak of the impurity observed.

B. Experimental results

Figure 1 shows a typical deuteron energy spectrum from the ^{96}Mo$(\vec{p},d)$ reaction at 8° (Laboratory angle). The overall energy resolution was about 40 keV [full width at half maximum (FWHM)] as shown in the Fig. 1 insertion. The energy calibration of the spectrum was performed by remapping some positions—which was done by adjusting the strength of the magnetic field—of well-known low-lying levels in ^{95}Mo, over a wide region in the spectrum, namely the ground state, 0.766, 0.821, 0.948, and 1.048 (average of 1.039 and 1.057) MeV [7]. From the relationship between the positions and the radii of curvature of the deuteron at some values of the magnetic field, a general formulation of energy calibration was obtained.

Discrete levels are distributed throughout the energy region up to an excitation energy of about 5 MeV, and the strongly excited states lie in the region below $\sim$3.5 MeV. The continuum spectrum region is found to exist in the relatively lower area starting from about 2 MeV. This comes from the spreading mechanism as we know that the spreading width and level density becomes large as a function of the energy measured from the Fermi surface [21]. The peaks were extracted from the spectrum using a peak fitting and peeling-off code, which provided good data reduction for a maximum of five peaks at a time. However, it is not desirable to fit all the peaks at a time, since the peak widths (FWHMs) observed in the spectrum change as a function of the excitation energy. So we used single search parameters for all the peak widths in a comparatively narrow region. But we had to extract for peaks at excitation energy 2.152, 2.188, and 2.223 MeV together because these peaks are too weak to own the resolution without referring to the neighbor peaks. Similarly for the peaks in the region above E_x=3.2 MeV or so, groups of weakly excited states with 2 to 5 peak elements and a continuum plateau are found, so that each group can be approached with a single parameter of peak resolution. Peaks located $E_x>5$ MeV were not analyzed because these are al-

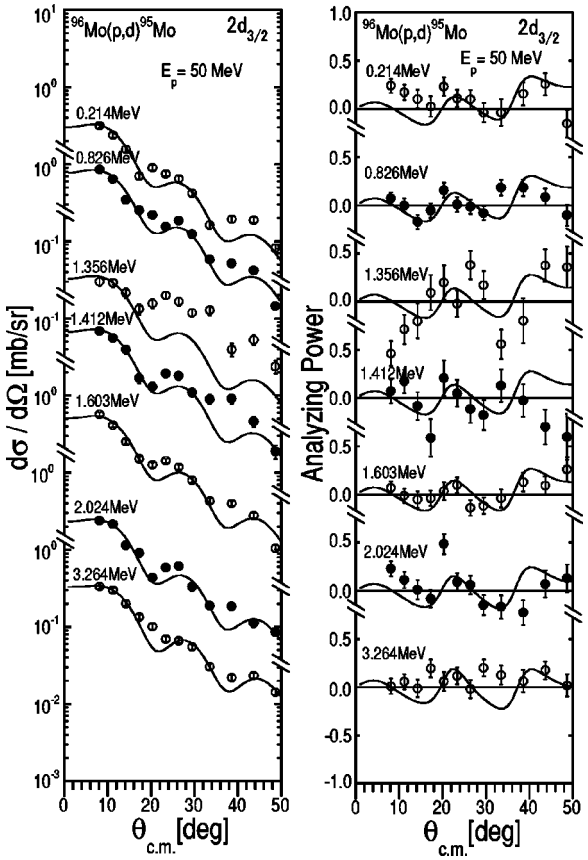

FIG. 2. Angular distribution of cross section (left) and analyzing powers (right) for the $3/2^+$ transitions in the ^{96}Mo$(p,d)^{95}$Mo reaction at 50 MeV.

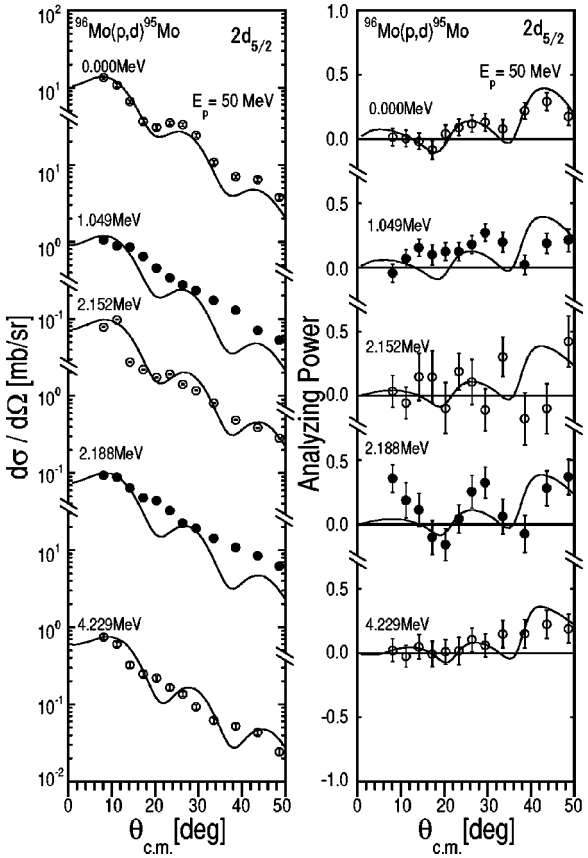

FIG. 3. Same as Fig. 2 for the $5/2^+$ transitions.

most covered by the background of continuum.

For a couple of weakly excited levels, namely at E_x = 3.698 and 3.741 MeV, the cross section data are not considered reliable, as these values were not satisfactorily reproduced in repeated extraction. Apart from these, the cross section data are extracted for all the remaining levels observed up to about E_x=5 MeV and DWBA analyses are carried out as discussed in the next section.

Angular distribution data for the analyzed states (both differential cross section and analyzing power) are shown in Figs. 2–7 together with the predictions of the DWBA theory using the optical parameter set listed in Table I. 51 levels were analyzed in the excitation region below 5 MeV and the transferred ℓj values were assigned for 49 levels. Results are summarized in Table II together with the results of Refs. [7] and [8].

III. DATA ANALYSES

A. Level to level analysis

The differential cross section and the corresponding analyzing power data are analyzed using the zero range DWBA code DWUCK-4 due to Kunz [26] under the local energy approximation model. The optical model potential was of the standard form as given by

$$V(r) = -Vf(x) - i\left(W - 4W_D a\frac{d}{dr}\right)f(x') + \left(\frac{\hbar}{m_\pi c}\right)^2 V_{so}\frac{1}{r}\frac{d}{dr}f(x'')\,l\,.\,s \qquad (1)$$

Here V, W, W_D, and V_{so} are the depths of various potentials and the corresponding form factors are

$$f(x) = [1 + \exp(r - R_R)/a_R]^{-1},$$

$$f(x') = [1 + \exp(r - R_W)/a_W]^{-1},$$

$$\text{and} \quad f(x'') = [1 + \exp(r - R_{so})/a_{so}]^{-1}, \qquad (2)$$

with $R_R = r_R A^{1/3}$, $R_W = r_W A^{1/3}$, and $R_{so} = r_{so} A^{1/3}$.

A coulomb term $V_c(r)$ due to uniformly charged spherical nucleus of radius $R_c = (r_c A^{1/3})$ was added to the earlier potential (1).

The different potential parameters are shown in Table I. For protons we used the global potential of Becchetti and Greenlees [27], while for deuterons an adiabatic potential [13] based on the proton and neutron potentials [27] were constructed, since it is known that such a combination of potentials is physically more meaningful than the best fit optical model potentials in the proton and deuteron channels [21]. The neutron bound-state wave functions were generated in a standard Woods-Saxon potential well with the geometrical parameters as given by r_n=1.25 fm and a_n=0.65 fm in-

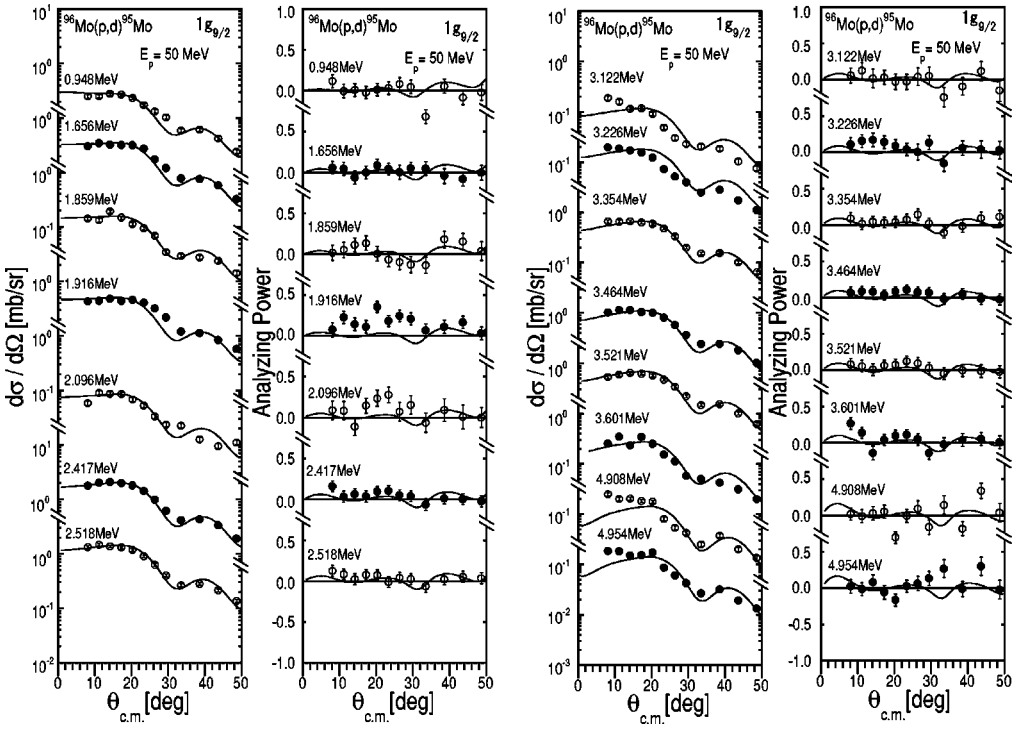

FIG. 4. Same as Fig. 2 for the $9/2^+$ transitions.

cluding a Thomas-Fermi spin-orbit term with the usual value $\lambda = 25$. The (real) well depth was adjusted to yield the neutron separation energy with the effective binding energy method.

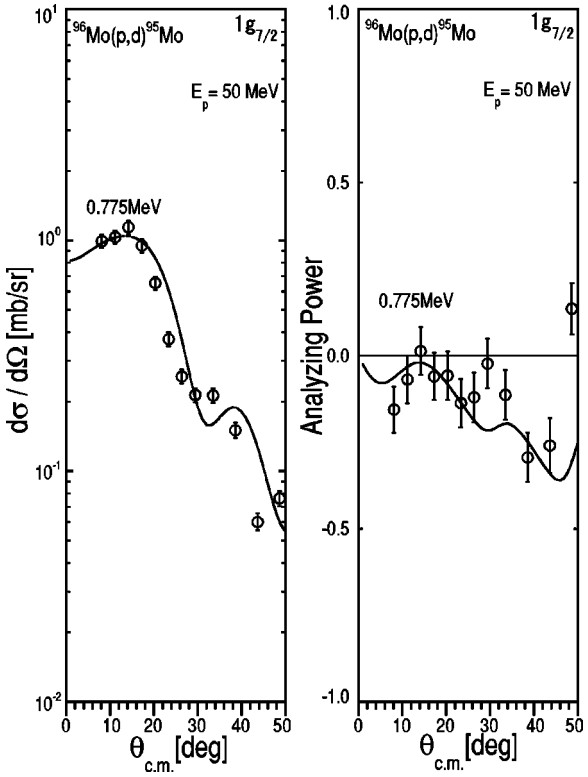

FIG. 5. Same as Fig. 2 for the $7/2^+$ transition.

In the local energy approximation model of DWBA, the finite range parameter of 0.621 was used and the nonlocality parameters were given the usual values of $\beta_p = \beta_n = 0.85$ fm and $\beta_d = 0.54$ fm. The spectroscopic factor C^2S for a transfer was obtained using the relation [26]:

$$\frac{d\sigma(\theta)}{d\Omega} = 2.30 \frac{C^2S}{2j+1} \left. \frac{d\sigma(\theta)}{d\Omega} \right|_{\mathrm{DWBA}}, \tag{3}$$

where $d\sigma(\theta)/d\Omega$ and $d\sigma(\theta)/d\Omega|_{\mathrm{DWBA}}$ are, respectively, the measured and the DWBA cross sections at the angle θ.

The DWBA fits to the measured cross sections and the corresponding analyzing powers $A_y(\theta)$ are illustrated in Figs. 2–7 and the results of the analyses are summarized in Table II. Also included in the Table II are the level properties of ^{95}Mo as summarized (i.e., the adopted values of the excitation energies of the levels and the corresponding J^π values), as well as the results given in the previous neutron pickup reactions on ^{96}Mo [8–12].

B. Continuum data analyses

In the present method, the theoretical calculations of the double differential cross sections have been done by considering a direct reaction model as an incoherent sum of the direct reaction components, which are based on DWBA predictions and expressed as follows:

$$\frac{d^2\sigma}{d\Omega dE} = 2.30 \sum_{\ell,j} \left\{ \frac{C^2S_{\ell,j}(E)}{2j+1} \times \left[\left. \frac{d\sigma}{d\Omega} \right|_{\ell,j}^{\mathrm{DW}} (E) \right] \right\}, \tag{4}$$

where $d\sigma/d\Omega|_{\ell,j}^{\mathrm{DW}}(E)$ is the cross section calculated by the DWBA code DWUCK [26] and $C^2S_{\ell,j}(E)$, the spectroscopic factor expressed as

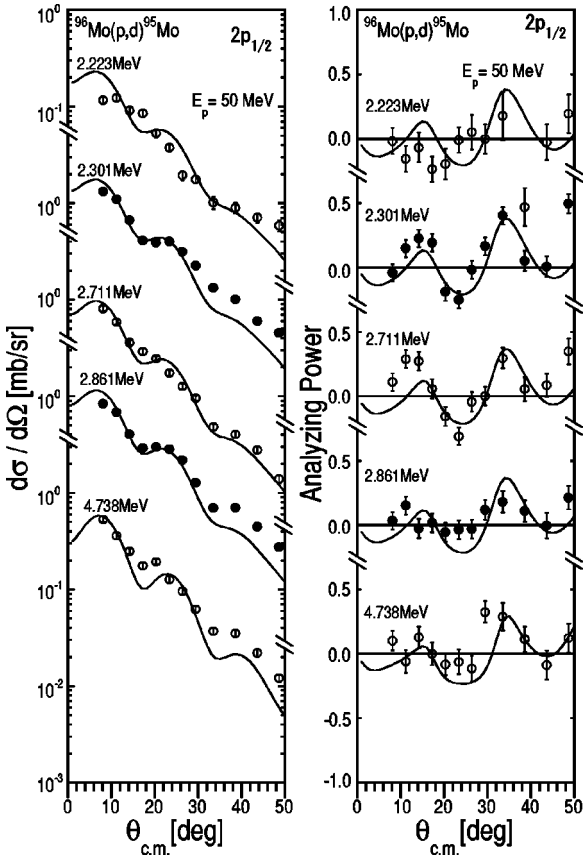

FIG. 6. Same as Fig. 2 for the $1/2^-$ transitions.

$$C^2S_{\ell,j}(E) = (\Sigma C^2S_{\ell,j}) \times f_{\ell,j}(E), \tag{5}$$

where $\Sigma C^2S_{\ell,j}$ is the sum of the spectroscopic factors of all the predicted states and the distribution of strength function over the spectra is obtained by using an asymmetric Lorentzian function [20,21,28]:

$$f_{\ell,j} = \frac{n_0}{2\pi} \frac{\Gamma(E)}{(|E - E_F| - E_{\ell,j})^2 + \Gamma^2(E)/4} \tag{6}$$

and

$$\int_0^\alpha f_{\ell,j}(E)dE = 1, \tag{7}$$

where n_0 is the renormalization constant and E_F is the Fermi energy. The Fermi energy can be calculated by using an empirical formula given in Ref. [14]. The sums of spectroscopic factors and the centroid energies $(E_{\ell,j})$ for $j = \ell \pm \frac{1}{2}$ shell orbits have been estimated by using Bardeen-Cooper-Schrieffer (BCS) calculations. In these calculations, single particle energies required to calculate the centroid energy are calculated by the prescription of Bohr and Mottelson [29]. The spreading width (Γ) is expressed by a function proposed by Brown and Rho [30] and by Mahaux and Sartor [28] as

$$\Gamma(E) = \frac{\epsilon_0(E - E_F)^2}{(E - E_F)^2 + E_0^2} + \frac{\epsilon_1(E - E_F)^2}{(E - E_F)^2 + E_1^2}, \tag{8}$$

where ϵ_0, ϵ_1, E_0, and E_1 are constants which express the effects of nuclear damping in the nucleus [20]. The estimated parameters [20] are

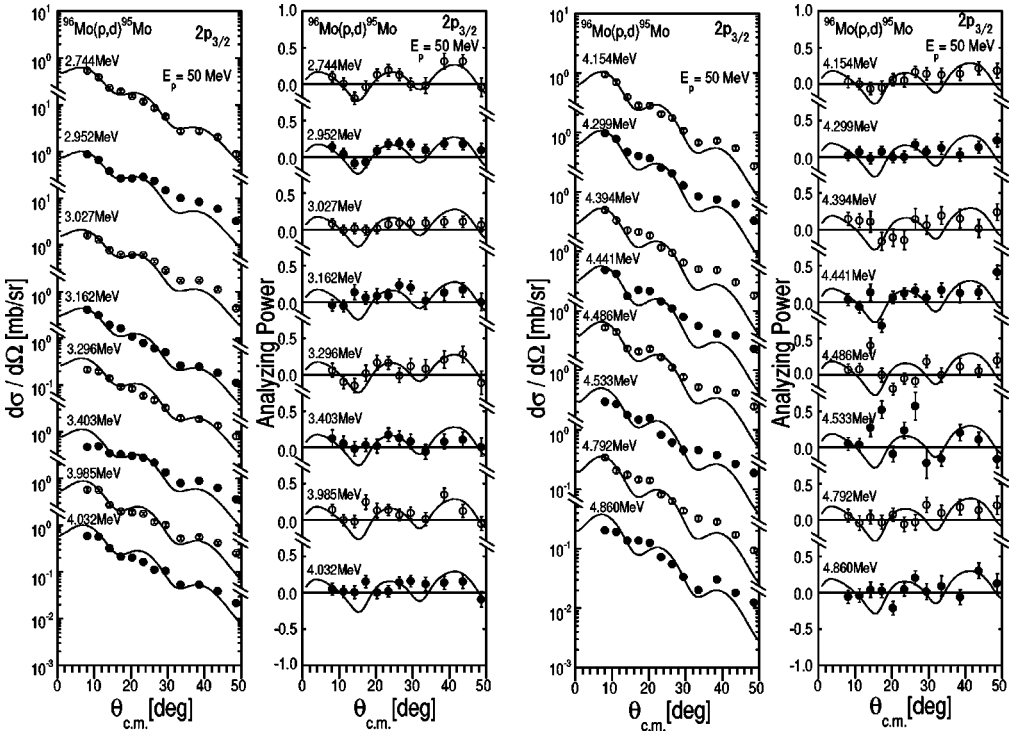

FIG. 7. Same as Fig. 2 for the $3/2^-$ transitions.

TABLE I. Optical model parameters used in the DWBA calculations.

Particle	V	r	a	r_c	W_v	W_s	r'	a'	V_{so}	r_{so}	a_{so}
	(MeV)	(fm)	(fm)	(fm)	(MeV)	(MeV)	(fm)	(fm)	(MeV)	(fm)	(fm)
Menet potential[a]											
Proton	45.87	1.16	0.75	1.25	5.70	3.64	1.37	0.47	6.04	1.06	0.78
Deuteron	[b]	1.16	0.75	1.25	[c]	[c]	1.37	[d]	6.04	1.06	0.78
Neutron	[e]	1.25	0.65								
Becchetti and Greenlees potential [f]											
Proton	44.66	1.17	0.75	1.25	8.30	0.80	1.31	0.60	6.20	1.01	0.75
Deuteron	[g]	1.17	0.78	1.25	[h]	[h]	1.29	0.62	6.20	1.06	0.75
Neutron	[i]	1.25	0.65								
Koning and Delaroche potential [j]											
Proton	37.73	1.22	0.66	1.24	5.16	4.98	1.27	0.53	4.94	1.04	0.59
Deuteron	[k]	1.22	0.66	1.24	[k]	[k]	1.27	0.55	[k]	1.04	0.59
Neutron	[l]	1.25	0.65		1.26						
	Nonlocality parameter (fm)				Finite-range parameter (fm)				Spin-orbit term $\lambda = 25$		
Proton	0.85				0.621						
Neutron	0.85				0.621						
Deuteron	0.54										

[a]See Ref. [25].
[b]$V = 99.8 - 0.44(E_d/2) + 0.4Z/A^{1/3}$(MeV).
[c]$W_v = 2.4 + 0.18(E_d/2)$(MeV), $W_s = 8.40 - 0.10(E_d/2)$(MeV), E_d is the deuteron kinetic energy.
[d]$a' = 0.74 - 0.008(E_d/2) + 1.0(N-Z)/2A$(fm).
[e]Well depth adjusted to fit the separation energy.
[f]See Ref. [27].
[g]$V = 110.3 - 0.64(E_d/2) + 0.4Z/A^{1/3}$(MeV).
[h]$W_v = 0.44(E_d/2) - 4.26$(MeV), $W_s = 24.8 - 0.50(E_d/2)$(MeV), E_d is the deuteron kinetic energy.
[i]Well depth adjusted to fit the separation energy.
[j]See Ref. [34].
[k]Adiabatic potentials with those of Ref. [34].
[l]Well depth adjusted to fit the separation energy.

$$\epsilon_0 = 19.4\ (\mathrm{MeV}), \quad E_0 = 18.4\ (\mathrm{MeV}),$$

$$\epsilon_1 = 1.40\ (\mathrm{MeV}), \quad E_1 = 1.60\ (\mathrm{MeV}). \tag{9}$$

The sum rule of the spectroscopic factors of nucleon orbits for $T \pm \frac{1}{2}$ isospin states are estimated with a simple shell model prescription [31]:

$$\sum C^2 S_{\ell,j} = \begin{cases} n_n(\ell,j) - \dfrac{n_p(\ell,j)}{2T+1} & \text{for} \quad T_< = T - \frac{1}{2} \\ \dfrac{n_p(\ell,j)}{2T+1} & \text{for} \quad T_> = T + \frac{1}{2} \end{cases}, \tag{10}$$

here $n_n(\ell,j)$ and $n_p(\ell,j)$ are the numbers of neutrons and protons respectively for each ℓ, j orbit and T is the isospin of the target nucleus.

IV. RESULTS AND DISCUSSION

A. General observation for discrete levels

The J^π values given from the present work are expected to be unambiguous for levels with a good fit simultaneously to both differential cross section and analyzing power. The angular distribution shapes as given by the DWBA for the $j = \ell + 1/2$ and $j = \ell - 1/2$ states are quite similar, but the analyzing powers show a clear distinction. Thus the uncertainties in the spin-parity assignment [7] should be considered as removed for many of the levels. The $\ell = 2$ transitions present difficulties, as the shapes of the analyzing power $A_y(\theta)$ given by the DWBA are quite similar to each other for the $d_{5/2}$ and $d_{3/2}$ transitions (Figs. 2 and 3). The only difference is that the minimum in $A_y(\theta)$ around 15° displayed in the latter only shifts to a somewhat larger angle in the former; this makes a few J^π assignment rather uncertain, namely those with a scatter in the experimental results. Unfortunately however the high level density of ^{95}Mo, in some of the cases, makes a one-to-one correspondence with the adopted levels somewhat difficult in particular for levels given from various nuclear reactions and β decays, for example, levels at $E_x = 2.024$, 2.096, 2.223 MeV. Such a problem does not arise for levels above $E_x = 3.2$ MeV or so, since the levels adopted [7] arise only from neutron pickup reactions, where the present work has a clear edge over similar previous studies but with unpolarized beams, while the high spin states ob-

TABLE II. Spectroscopic results from neutron pickup reactions on ^{96}Mo. (a) Present Work. Doubtful assignments are shown in parenthesis. (b) Adopted values, from Ref. [7] (c) Bindal *et al.* (See Ref [8]). (d) Range of spectroscopic factors from pickup (one neutron) reactions on ^{96}Mo (See Refs. [8–12]) other than those already presented in this table.

E_x(MeV)			ℓ		J^π			C^2S		
(a)	(b)	(c)	(a)	(c)	(a)	(b)	(c)	(a)	(c)	(d)
0.000	0.000	0.000	2	2	$\frac{5}{2}^+$	$\frac{5}{2}^+$	$\frac{5}{2}^+$	1.663	1.980	1.700–3.900
0.214_3	0.204_{18}	0.201_6	2	2	$\frac{3}{2}^+$	$\frac{3}{2}^+$	$\frac{3}{2}^+$	0.044	0.050	0.040–0.100
0.775_3	0.766_7	0.769_6	4	4	$\frac{7}{2}^+$	$\frac{7}{2}^+$	$\frac{7}{2}^+$	0.813	(0.880)	0.450–0.890
	0.786_{25}					$\frac{1}{2}^+$				
0.826_2	0.821_5	0.816_7	2	2	$\frac{3}{2}^+$	$\frac{3}{2}^+$	$\frac{3}{2}^+$	0.115	0.160	0.140–0.212
0.948_2	0.948_{15}	0.945_7	4	4	$\frac{9}{2}^+$	$\frac{9}{2}^+$	$\frac{9}{2}^+$	0.152	0.260	0.180–0.334
	1.039_4					$\frac{1}{2}^+$				
1.049_4	1.057_{14}	1.044_{10}	(2)	2	$(\frac{5}{2}^+)$	$\frac{5}{2}^+$	$\frac{5}{2}^+$	(0.150)	0.180	0.100–0.186
	1.074_{13}					$\frac{7}{2}^+$				
	1.092_{12}	1.092_{12}		4+2		$\frac{3}{2}^+, \frac{5}{2}^+$	$(\frac{7}{2}^+, \frac{5}{2}^+)$		0.060(4),0.040(2)	
	1.303_{10}					$\frac{1}{2}^+$				
	1.322_7					$(\frac{3}{2}^+, \frac{5}{2}^+)$				
1.356_9	1.370_{14}	1.367_{15}	2	1	$(\frac{3}{2})^+$	$(\frac{3}{2})$	$\frac{1}{2}^-$	(0.005)	0.020	
	1.376_{20}					+				
1.412_7	1.426_3	1.428_{12}	2	2	$\frac{3}{2}^+$	$(\frac{5}{2})^+$	$\frac{3}{2}^+$	0.010	0.014	0.014–0.019
	1.440_3					$(\frac{7}{2}^+, \frac{9}{2}, \frac{11}{2})$				
	1.541_{12}	1.542_{10}		4		$\frac{11}{2}^+$	$\frac{9}{2}^+$		0.034	
	1.552_{16}					$(\frac{9}{2})^+$				
1.603_3	1.620_3	1.618_{10}	2	2	$\frac{3}{2}^+$	$\frac{3}{2}^+$	$\frac{3}{2}^+$	0.078	0.079	0.084–0.125
	1.645_7					$\frac{7}{2}^{(+)}$				
	1.660_{25}					$(\leqslant\frac{5}{2})$				
1.656_2	1.666_8	1.674_{10}	4	4	$\frac{9}{2}^+$	$(\frac{7}{2}^+, \frac{9}{2}^+)$	$\frac{9}{2}^+$	0.217	0.350	0.190–0.310
	1.683					$\frac{7}{2}, \frac{9}{2}^{(+)}$				
	1.698_{10}					$\frac{1}{2}^+$				
	1.743_{16}					$(\frac{9}{2})$				
	1.797_{18}									
	1.808_{22}					$(\frac{7}{2}^+)$				
1.859_3	1.879_{12}	1.879_{12}	4	4	$\frac{9}{2}^+$	$(\frac{9}{2}^+)$	$\frac{9}{2}^+$	0.098	0.110	0.084
1.916_5			4		$(\frac{9}{2})^+$			(0.315)		
	1.938_{22}	1.942_{12}		5+2		$\frac{11}{2}^-$	$\frac{11}{2}^-, \frac{5}{2}^+$		0.330(5),0.033(2)	
	1.963					$\frac{3}{2}^+, \frac{5}{2}^+$				
	1.984_{15}	1.984_{15}		2		$\frac{3}{2}^+, \frac{5}{2}^+$	$\frac{5}{2}^+$		(0.024)	
	(2.049)					$\frac{1}{2}^+$				
2.024_4	2.050_{15}	2.050_{15}	2	2	$\frac{3}{2}^+$	$(\frac{3}{2})^+$	$\frac{3}{2}^+$	0.037	0.030	0.040
	2.059_{19}					$\frac{13}{2}(+)$				
	2.067					$(\frac{5}{2}^-, \frac{7}{2}^-)$				
	2.089					$(\frac{3}{2})^+$				
2.096_7	2.130_{15}	2.130_{15}	4	4	$\frac{9}{2}^+$	$\frac{7}{2}^+, \frac{9}{2}^+$	$\frac{9}{2}^+$	0.054	0.060	
2.152_9			(2)		$(\frac{5}{2}^+)$			(0.130)		
2.188_5	2.179_{15}	2.179_{15}	2	2	$\frac{5}{2}^+$	$(\frac{3}{2})^+$	$\frac{3}{2}^+$	0.013	0.020	
	2.212_4					$\frac{1}{2}^-, \frac{3}{2}^-$				
2.223_6	2.233_4	2.240_{15}	1	1+2	$(\frac{1}{2})^-$	$(\frac{15}{2})^+$	$\frac{1}{2}^-, \frac{5}{2}^+$	(0.041)	0.030(1),0.040(2)	0.027–0.030

TABLE II. (*Continued.*)

E_x(MeV)			ℓ		J^π			C^2S		
(a)	(b)	(c)	(a)	(c)	(a)	(b)	(c)	(a)	(c)	(d)
	2.252					$(\frac{3}{2})^+$				
2.301_2	2.315_8	2.319_{12}	1	1	$\frac{1}{2}^-$	$\frac{1}{2}^-, \frac{3}{2}^-$	$\frac{1}{2}^-$	0.315	0.330	0.180–0.370
	2.357					$\frac{1}{2}^+$				
	2.383	2.375_{15}		0+2		$(\frac{3}{2})^+$	$\frac{1}{2}^+, \frac{5}{2}^+$		[0.130(0)],[0.050(2)]	
	2.396_{10}					$(\frac{3}{2})^+$				
2.417_2	2.428_{13}	2.441_{12}	4	4	$\frac{9}{2}^+$	$\frac{7}{2}^+, \frac{9}{2}^+$	$\frac{9}{2}^+$	1.359	1.810	1.300–2.100
	2.490_{20}					$(\frac{3}{2})^+$				
	2.501_{15}	2.501_{15}		(4)		$(\frac{7}{2}^+, \frac{9}{2}^+)$	$\frac{9}{2}^+$		(0.180)	
2.518_2	2.531_{12}	2.531_{12}	4	4	$\frac{9}{2}^+$	$\frac{7}{2}^+, \frac{9}{2}^+$	$\frac{9}{2}^+$	0.978	1.180	0.880–1.380
	2.544					$(\frac{1}{2}^-, \frac{3}{2}^-)$				
	2.581_3					$(\frac{17}{2})^+$				
	2.602					$\frac{1}{2}^+$				
	2.612_{18}									
	2.671									
	2.695					$(\frac{3}{2}^+)$				
2.711_3	2.718_{15}	2.718_{15}	1	1	$\frac{1}{2}^-$	$\frac{1}{2}^-, \frac{3}{2}^-$	$\frac{1}{2}^-$	0.174	0.220	0.150
	2.725					$(\frac{3}{2}^+)$				
	2.732_4					$(+)$				
2.744_4	2.745		1		$\frac{3}{2}^-$	$(\frac{3}{2}^+)$		0.109		
	2.769_{15}	2.769_{15}		1		$\frac{1}{2}^-, \frac{3}{2}^-$	$\frac{1}{2}^-$		0.130	
	2.830					$(\frac{3}{2})^+$				
	2.843					$(\frac{3}{2})^+$				
2.861_3	2.890_{15}	2.890_{15}	1	1	$\frac{1}{2}^-$	$\frac{1}{2}^-, \frac{3}{2}^-$	$\frac{1}{2}^-$	0.207	0.180	0.120
2.952_3	2.986_{17}	2.986_{17}	1	1	$\frac{3}{2}^-$	$\frac{1}{2}^-, \frac{3}{2}^-$	$\frac{1}{2}^-$	0.174	0.170	
3.027_3	3.037		1		$\frac{3}{2}^-$	$(\frac{3}{2})^+$		0.370		
	3.063_{17}	3.063_{17}		1		$\frac{1}{2}^-, \frac{3}{2}^-$	$\frac{1}{2}^-$		0.350	
3.122_5	3.142		4		$\frac{9}{2}^+$	$(\frac{3}{2})^+$		0.087		
3.162_4	3.170_{20}	3.170_{20}	1	2	$(\frac{3}{2})^-$	$\frac{3}{2}^+, \frac{5}{2}^+$	$\frac{3}{2}^+$	(0.076)	0.060	
3.226_3	3.200_{20}	3.200_{20}	4	(2)	$\frac{9}{2}^+$	$(\frac{3}{2}^+, \frac{5}{2}^+)$	$\frac{3}{2}^+$	0.136		
3.264_4	3.260_{20}	3.260_{20}	2	2	$(\frac{3}{2})^+$	$\frac{3}{2}^+, \frac{5}{2}^+$	$\frac{3}{2}^+$	(0.057)	0.070	0.070
3.296_6	3.310_{20}	3.310_{20}	1	2	$\frac{3}{2}^-$	$\frac{3}{2}^+, \frac{5}{2}^+$	$\frac{3}{2}^+$	0.065	0.040	
	$(3.310)_{10}$					$(\frac{7}{2}^+, \frac{9}{2}^+)$				
3.354_3		3.380_{17}	4	4	$\frac{9}{2}^+$		$\frac{9}{2}^+$	0.511	0.590	0.360
3.403_5	3.395_{15}	3.443_{17}	1	1	$\frac{3}{2}^-$	$\frac{7}{2}^+, \frac{9}{2}^+$	$\frac{1}{2}^-$	0.196	0.200	0.200–0.210
3.464_2	3.443_{17}	3.494_{17}	4	4	$\frac{9}{2}^+$	$\frac{1}{2}^-, \frac{3}{2}^-$	$\frac{9}{2}^+$	0.870	1.00	0.810–0.990
	3.506_9					$\frac{7}{2}^+, \frac{9}{2}^+$				
3.521_3	3.551_{17}	3.551_{17}	4	4	$\frac{9}{2}^+$	$\frac{7}{2}^+, \frac{9}{2}^+$	$\frac{9}{2}^+$	0.544	0.650	0.250–0.630
3.601_4	3.625_{17}	3.625_{17}	4	4	$\frac{9}{2}^+$	$\frac{7}{2}^+, \frac{9}{2}^+$	$\frac{9}{2}^+$	0.213	0.310	0.330
	3.635_5					$(+)$				
3.698_{13}										
3.741_{16}										
3.985_8	3.960_{20}	3.960_{20}	1	1	$\frac{3}{2}^-$	$\frac{1}{2}^-, \frac{3}{2}^-$	$\frac{3}{2}^-$	0.152	0.084	0.065
4.032_6	4.010_{20}	4.010_{20}	1	1	$(\frac{3}{2})^-$	$\frac{1}{2}^-, \frac{3}{2}^-$	$\frac{3}{2}^-$	(0.174)	0.140	0.120
	4.070_{20}	4.070_{20}		1		$\frac{1}{2}^-, \frac{3}{2}^-$	$\frac{3}{2}^-$		0.150	

TABLE II. (*Continued.*)

E_x(MeV)			ℓ		J^π			C^2S		
(a)	(b)	(c)	(a)	(c)	(a)	(b)	(c)	(a)	(c)	(d)
4.154_6	4.170_{20}	4.170_{20}	1	1	$\frac{3}{2}^-$	$\frac{1}{2}^-,\frac{3}{2}^-$	$\frac{3}{2}^-$	0.180	0.130	0.110
4.229_6	4.240_{20}	4.240_{20}	2	1	$\frac{5}{2}^+$	$\frac{1}{2}^-,\frac{3}{2}^-$	$\frac{3}{2}^-$	0.117	0.120	
4.299_6	4.310_{20}	4.310_{20}	1	1	$(\frac{3}{2})^-$	$\frac{1}{2}^-,\frac{3}{2}^-$	$\frac{3}{2}^-$	(0.184)	0.120	0.110
4.394_{17}	4.350_{20}	4.350_{20}	1	1	$(\frac{3}{2})^-$	$\frac{1}{2}^-,\frac{3}{2}^-$	$\frac{3}{2}^-$	(0.091)	0.140	0.060
4.441_{17}	4.400_{25}	4.400_{25}	1	1	$\frac{3}{2}^-$	$\frac{1}{2}^-,\frac{3}{2}^-$	$\frac{3}{2}^-$	0.098	0.090	0.080
4.486_{17}	4.450_{25}	4.450_{25}	1	1	$(\frac{3}{2})^-$	$\frac{1}{2}^-,\frac{3}{2}^-$	$\frac{3}{2}^-$	(0.113)	0.140	0.080
4.533_{19}	4.500_{25}	4.500_{25}	1	1	$(\frac{3}{2})^-$	$\frac{1}{2}^-,\frac{3}{2}^-$	$\frac{3}{2}^-$	(0.087)	0.130	0.090
	4.560_{20}	4.560_{30}		2		$\frac{3}{2}^+,\frac{5}{2}^+$	$\frac{3}{2}^+$		0.030	
	4.630_{30}	4.630_{30}		(2)		$(\frac{3}{2}^+,\frac{5}{2}^+)$	$\frac{3}{2}^+$		(0.020)	
4.738_{12}	4.740_{30}	4.740_{30}	1	1	$\frac{1}{2}^-$	$\frac{1}{2}^-,\frac{3}{2}^-$	$\frac{3}{2}^-$	0.105	0.080	0.050
4.792_{13}	4.810_{30}	4.810_{30}	1	1	$(\frac{3}{2})^-$	$\frac{1}{2}^-,\frac{3}{2}^-$	$\frac{3}{2}^-$	(0.061)	0.040	0.030
4.860_{12}			1		$(\frac{3}{2})^-$			(0.065)		
4.908_{16}			4		$(\frac{9}{2})^+$			(0.136)		
4.954_{24}			4		$\frac{9}{2}^+$			0.136		

served in gamma decay studies following heavy ion induced reactions [32,33] are not expected to be populated in the single step neutron pickup reactions obviously because of their rather complicated configurations.

As stated earlier DWBA analyses were carried out for all but a couple of levels and the ℓ,j transfers and spectroscopic factors are extracted (Table II). The reliability of the C^2S values was tested by using two other global potentials for protons [25,34] and the corresponding adiabatic potential for deuterons. These potentials are also shown in Table I. Sample DWBA analyses were carried out using these potential sets for transitions at least one each to the shell model states given by $2d_{5/2}$(E_x=0.00 MeV), $1g_{7/2}$(E_x=0.775 MeV), $2d_{3/2}$(E_x=1.603 MeV), $2p_{1/2}$(E_x=2.301 MeV), $1g_{9/2}$(E_x=2.417 MeV), $1g_{9/2}$(E_x=2.518 MeV), $2p_{1/2}$(E_x=2.861 MeV), $2p_{3/2}$(E_x=2.952 MeV), $2p_{3/2}$(E_x=3.027 MeV), and $1g_{9/2}$(E_x=3.464 MeV). Fits are shown in Figs. 8 and 9 and the corresponding spectroscopic factors are given in Table III. These values are consistent to one another for all three combinations of potentials within the uncertainties arising from the measurement of the absolute cross section and the normalization of the DWBA to experiment. Further to the ℓj transfer (i.e., assignment of the J^π value), the spectroscopic factors given in Table II should therefore be considered as reliable and hence meaningful.

B. Level to level observation

(i) Except for a doubtful ℓ_n=3 assignment made in a ^{96}Mo(d,t) reaction [11], which is also adopted [7], in no other neutron pickup reactions on ^{96}Mo was any ℓ=3 transition observed [8–10,12] and in the present work also, even though both $2p_{1/2}$ and $2p_{3/2}$ transitions are clearly seen over a wide range of excitation energy (Table II). Similar fragmentation of the $1f_{5/2}$ shell model strength in a neutron pickup reaction is perhaps not unexpected, because this shell model state is known to be quite close to the $2p_{1/2}$ state in many nuclei and one or more of the possible components of the $1f_{5/2}$ shell should have been present in the excitation energy covered in our study (E_x up to about 5 MeV).

We now look into the situation on neutron pickup reactions carried out on other Mo isotopes, namely ^{92,94,100}Mo [8,14,15,35], having the number of neutrons on either side of that in the present work above the neutron magic number of 50. Quite a few ℓ=3 transitions, including tentative ones, to $1f_{5/2}$ and even $1f_{7/2}$ states, are indeed observed in the ^{92}Mo$(\vec{p},d)$ reaction [14]. A few ℓ_n=3 transitions is observed in the (d,t) reaction on ^{94}Mo [8]. A very low-lying level, E_x=1.022 MeV, is found in the ^{100}Mo$(\vec{p},d)$ reaction [35] with angular distributions characteristic of the ℓ=3 transfer. Even though the j value is uncertain, because an unpolarized beam was used, the ℓ_n value is certainly quite convincing. As against this, neither this nor any other ℓ=3 transition is found in the $(\vec{p},d)$ reaction on ^{100}Mo [15]. Summing up, the situation for the earlier transitions exciting the $1f$ shell model state is far from clear.

(ii) A low-lying ℓ=5 transition to the 1.94 MeV level in ^{95}Mo observed in previous neutron pickup reactions on ^{96}Mo [8,11,12] is not excited in the present investigation with a measurable yield. Population of such a level in a single-step neutron pickup reaction would mean a highly diffuse Fermi surface. This is not supported in our study and if the level is at all excited, it should be certainly through a nonsingle step process.

(iii) The ℓ transfer, hence also the j transfer, given in the previous neutron pickup reactions on ^{96}Mo, namely to the levels at E_x=1.356, 3.162, 3.226, 3.296, and 4.229 MeV, are contradicted in our study (Table II). The DWBA fits to both differential cross section and analyzing power to all these levels, except perhaps the 1.356 and 3.162 MeV levels, are

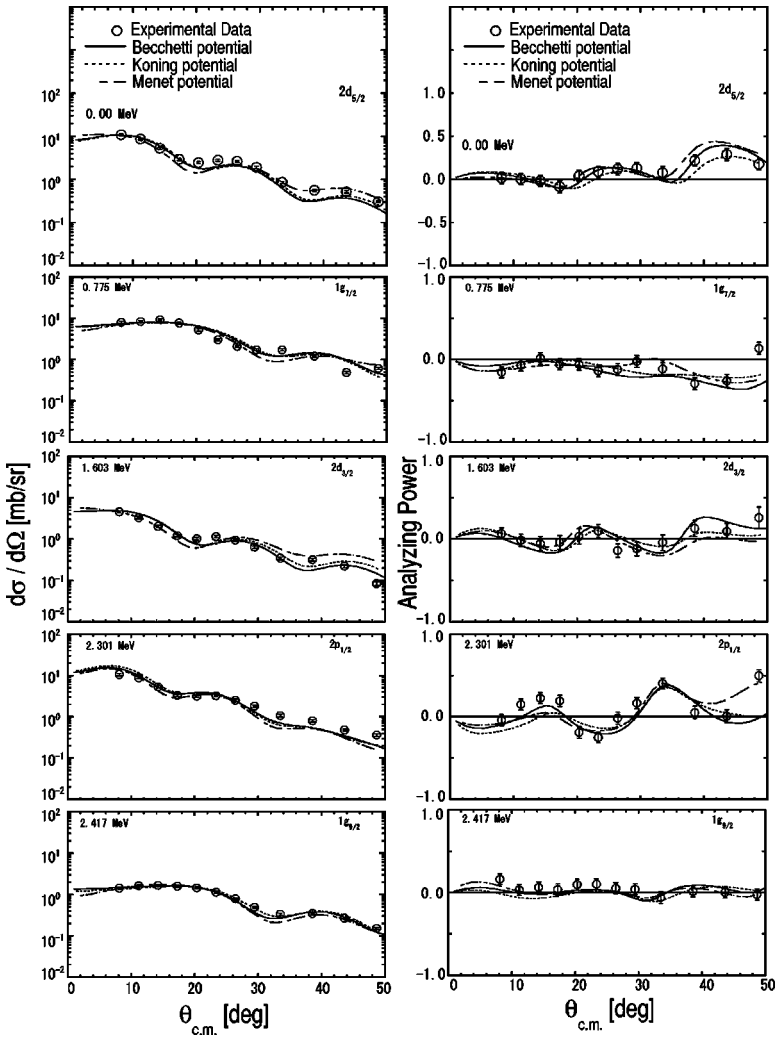

FIG. 8. Comparison of differential cross section and analyzing power for different potentials at $E_x = 0.00$, 0.775, 1.603, 2.301, and 2.417 MeV.

quite satisfactory to support the assignment of ℓj transfer made in the present work. The 1.356 MeV level is weakly populated and therefore the cross section data are not considered to be accurate. For the 3.162 MeV level the fit to the angular distribution is certainly characteristic of the $\ell = 1$ transfer (Fig. 7) thus disagreeing with the previous $\ell = 2$ assignment, even though the analyzing power data having a great deal of scatter are not well reproduced.

(iv) Some levels in ^{95}Mo, not hitherto observed, namely at $E_x = 1.916$, 2.152, 4.860, 4.908, and 4.954 MeV, are excited in the present experiment. Of these, a reliable assignment of J^π values could be made for the 4.954 MeV level, while for the others the J^π assignments are not unique in view of a poor fit to one or the other of the measured $d\sigma/d\Omega$ or A_y. For the other four levels assignments are shown in parenthesis. For a couple of levels excited at $E_x = 3.698$ and 3.741 MeV no J^π assignment is possible.

(v) A few $1/2^+$ levels are known to exist in ^{95}Mo at low excitation [7], none of which is populated in the present work with at least any measurable cross sections. This is understood as due to the fact that the $3s_{1/2}$ shell model state lies much above the Fermi surface, while the $2s_{1/2}$ state, being very deep lying, may appear only at high excitation energies. These $1/2^+$ levels are further more populated in the ^{94}Mo(d,p) stripping reaction [36], thereby suggesting that these belong to the $3s_{1/2}$ shell model state. No clear picture, however, emerges from previous studies of the neutron pickup reactions on ^{96}Mo. A couple of very low lying levels, namely $E_x = 0.786$ and 1.039 MeV, are populated in some of these studies with fairly large cross sections [9–11], but not in the others [8,12], while the 2.357 MeV level was observed by Bindal *et al.* [8] only in the (p,d) reaction, but not in the (d,t) reaction, nor was it observed in other single neutron pickup reactions on ^{96}Mo [9–12].

C. Sum rule analyses

Summation of the spectroscopic factors of the $1g_{9/2}$, $2p_{1/2}$, $2p_{3/2}$, $1g_{7/2}$, $2d_{5/2}$, $2d_{3/2}$, and $1h_{11/2}$ orbits for single-hole states from neutron pickup reaction on ^{96}Mo are presented in Table IV together with results of Bindal *et al.* [8] and simple shell model predictions. In the summation process of the spectroscopic factors, some data for which the assignment of transferred j values is ambiguous (cited in parentheses) are included, because of their weak effects on the final results.

Although the absolute values of the spectroscopic factors have systematic errors arising, for example, from the optical

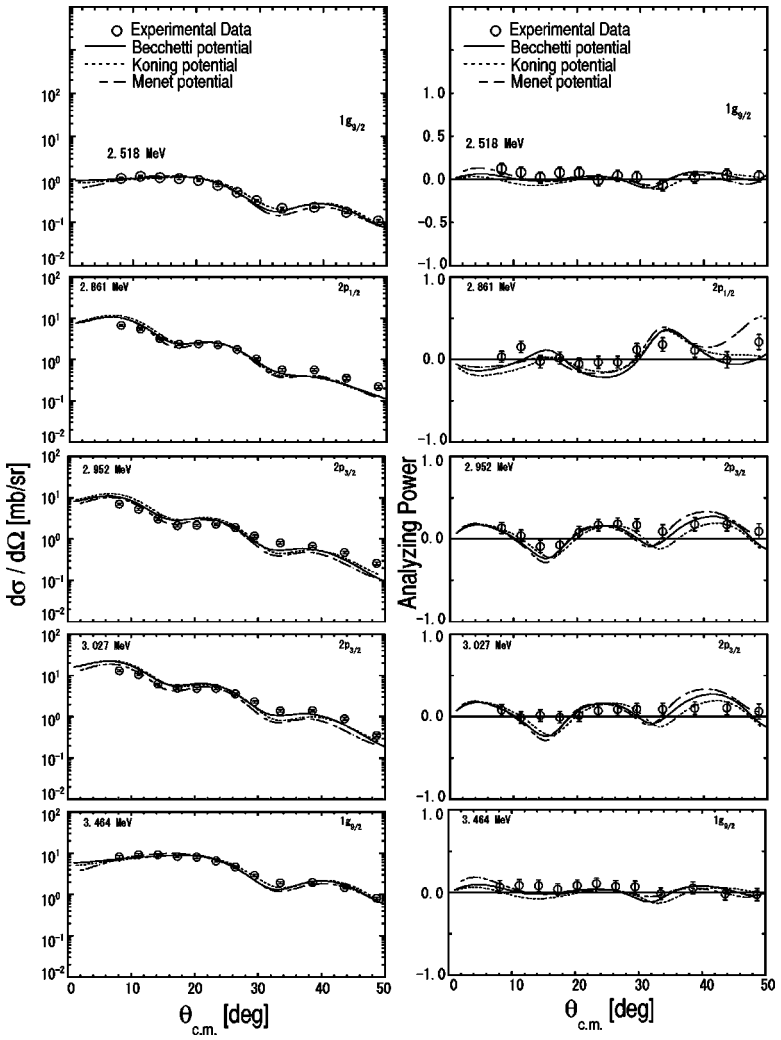

FIG. 9. Same as Fig. 8 for E_x=2.518, 2.861, 2.952, 3.027, and 3.464 MeV.

model and bound-state parameters for DWBA analysis, it is important to compare results with the sum-rule limit because the data are always useful to discuss the quenching phenomena in the nuclear structure response.

The sums of the spectroscopic factors of neutron orbits for $T\pm\frac{1}{2}$ isospin states above a closed shell core are estimated with a simple shell model prescription described in Eq. (10), i.e.:

TABLE III. Comparison of spectroscopic factors for different potentials. (a) Becchetti and Greenlees (See Ref. [27]). (b) Menet *et al.* (See Ref. [25]). (c) Koning and Delaroche (See Ref. [34]).

Orbit	E_x (MeV)	C^2S (MeV) (a)	(b)	(c)
$2d_{5/2}$	0.000	1.66	1.76	1.63
$1g_{7/2}$	0.775	0.81	0.81	0.81
$2d_{3/2}$	1.603	0.078	0.083	0.078
$2p_{1/2}$	2.301	0.32	0.30	0.33
$1g_{9/2}$	2.417	1.36	1.52	1.36
$1g_{9/2}$	2.518	0.98	1.09	0.98
$2p_{1/2}$	2.861	0.21	0.20	0.22
$2p_{3/2}$	2.952	0.17	0.20	0.17
$2p_{3/2}$	3.027	0.37	0.40	0.35
$1g_{9/2}$	3.464	0.87	0.98	0.87

TABLE IV. Summed spectroscopic factors. (a) Present work. (b) Bindal *et al.* (See Ref. [8]).

Orbit	Experiment (a)	Experiment (b)	Simple shell model prediction
$1g_{9/2}$	5.81	6.53	
$2p_{1/2}$	0.84	1.63	20.92
$2p_{3/2}$	2.20	1.36	
$1g_{7/2}$	0.81	0.94	
$2d_{5/2}$	2.07	2.35	4.00
$2d_{3/2}$	0.35	0.57	
$1h_{11/2}$		0.33	
$3s_{1/2}$		0.13	
Subtotal	12.08	13.84	24.92

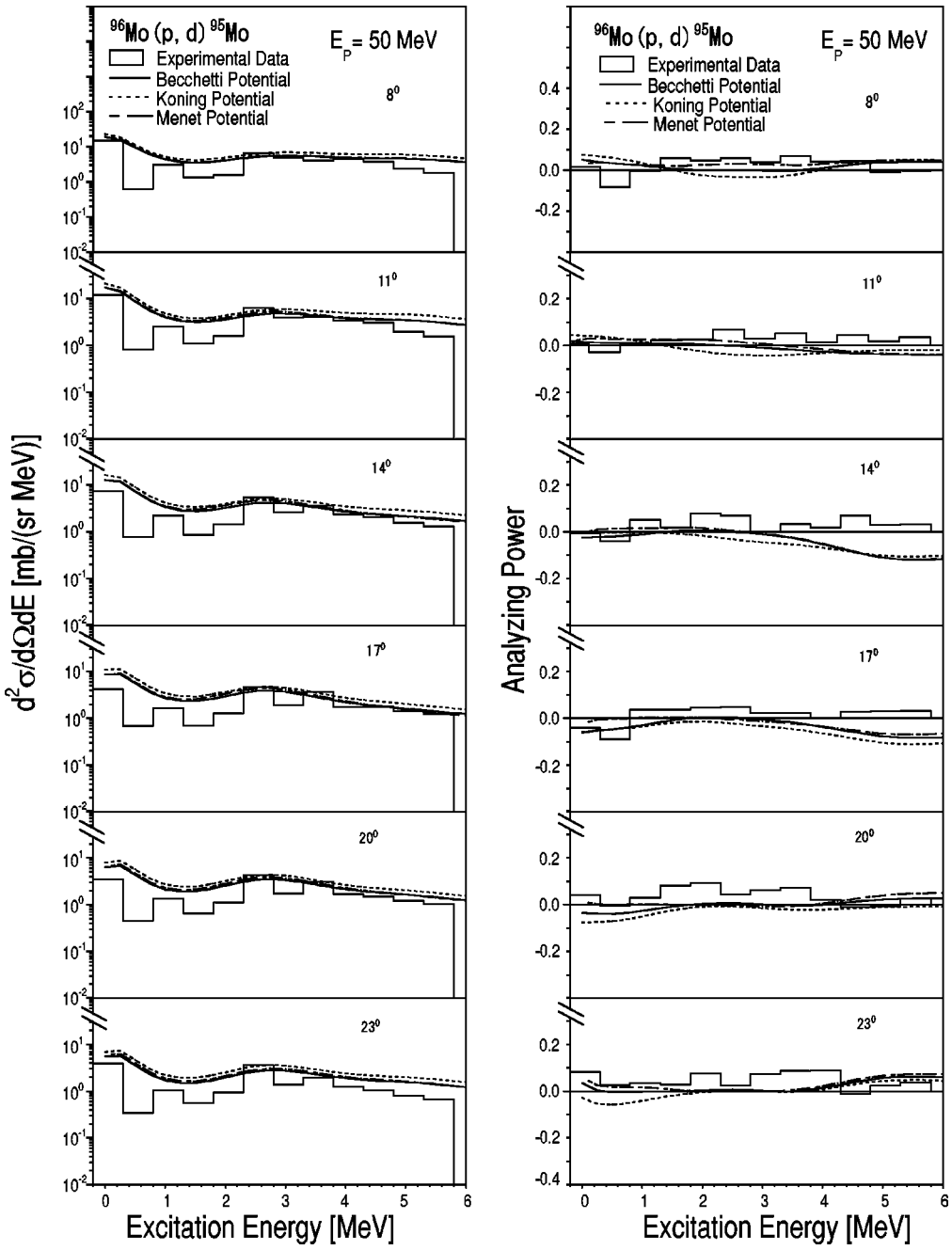

FIG. 10. Double differential cross section (left) and analyzing powers (right) obtained for the ^{96}Mo$(p,d)^{95}$Mo reaction at 50 MeV.

$$\sum C^2S_{\ell,j} = \begin{cases} n_n(\ell,j) - \dfrac{n_p(\ell,j)}{2T+1} & \text{for} \quad T_< = T - \frac{1}{2} \\ \dfrac{n_p(\ell,j)}{2T+1} & \text{for} \quad T_> = T + \frac{1}{2} \end{cases},$$

where n_n and n_p are the numbers of neutrons and protons, respectively, above the closed shell core and T is the target isospin. We assume here 28 as the closed shell core for ^{96}Mo, i.e., n_p=14 and n_n=26 and T=6, then the sum rule limits of $\Sigma C^2S = 20.92(1g_{9/2}+2p_{1/2}+2p_{3/2}) + 4.00(1g_{7/2}+2d_{5/2}+2d_{3/2}) = 24.92$.

Results of the sum rule analyses are summarized in Table IV. Since the isobaric analog of the ground state of ^{95}Mo is at E_x=12.2 MeV, the analog states are not populated within the excitation energy covered in the present work and these $T_>$ strengths are not included in the table. Because of the well known fragmentation of the single particle strengths it is certainly possible that levels beyond E_x=5.8 MeV should carry some of the strengths quoted in the table. The summed strengths obtained in the present work and by Bindal *et al.* [8] are close to each other for all but the $2p_{1/2}$ and $2p_{3/2}$ shell model states, the present values being smaller for the former state and larger for the latter. Simultaneous good fits to $d\sigma/d\Omega$ and A_y should make the present values reliable. The

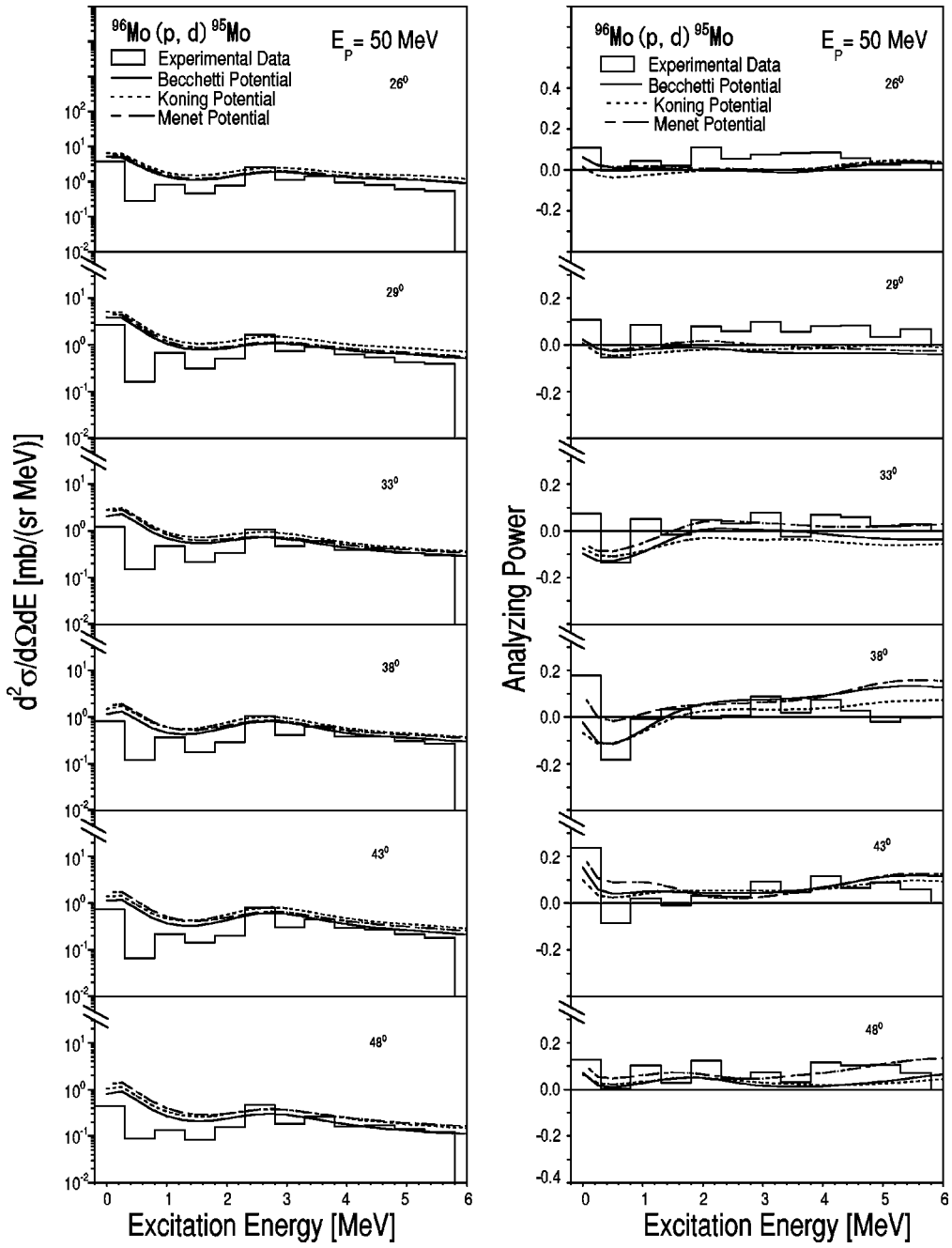

FIG. 11. Same as Fig. 10 but for different angles.

transitions to the $1h_{11/2}$ and $3s_{1/2}$ shell model states found by Bindal *et al.* are not observed in the present study. Their excitation through a single step process is somewhat surprising as these are much above the Fermi surface. This point is discussed in Sec. IV B. Taking all the points discussed earlier into acount, the sum of the spectroscopic factors determined in the present works are consistent with those of Bindal *et al.* [8] and has a significant role for understanding nuclear structure.

D. Continuum spectra analyses

(i) In the present study, we analyzed the measured energy spectra by overlapping the DWBA predictions as described earlier in Sec. III B. The prescription of Bohr and Mottelson [29] which is modified to fit the ^{40}Ca single-hole states deduced by Nedjadi *et al.* [37] was used to calculate the single particle energies. The values of Fermi energies for neutron $E_F(n)$ and proton $E_F(p)$, separation energies for neutron S_n and proton S_p of ^{96}Mo, respectively, -7.9738, -6.9377, 9.1542, and 9.2974 were used here. From the BCS theory, we can understand that only shell orbits from $1g_{9/2}$, $2p_{3/2}$ of $T_<$ have significant effects in giving the shape of the spectrum below 5.8 MeV, while the elements of $T_>$ do not have any effect because the isobaric analog ground state $E_{T>}$ of ^{95}Mo is known as the level at 12.2 MeV.

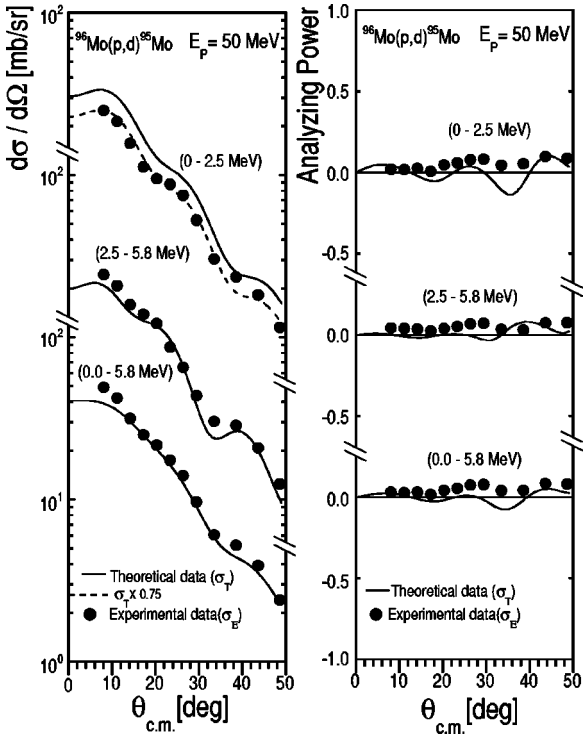

FIG. 12. Angular distributions of the summative cross sections (left) and analyzing powers in the ^{96}Mo$(p,d)^{95}$Mo reaction at 50 MeV. Solid curves refer to the predictions due to the present analysis, dotted curve the predictions after normalized to fit the experimental results. The normalization coefficients is 0.75 for the 0–2.5 MeV region.

We used here three global potentials for protons [25,27,34] and the corresponding adiabatic potentials for deuterons to analyze the double differential cross section (DDX) spectra and the results for the cross section and analyzing powers are consistent with one another as shown in Figs. 10 and 11. The different potential parameters are shown in Table I. The measured energy spectra of DDX and analyzing powers were converted to 500 keV wide energy spectra. Figures 10 and 11 show double differential energy for laboratory angles of $8°-48°$, with lines representing the theoretical cross sections and analyzing powers, and histograms the experimental ones. The present calculated values (theoretical) for angular distributions of double differential cross sections are overstimated a little at lower excitation energy in magnitude; however, for analyzing power, it is generally understimated a little up to angle 29°. The direction of analyzing powers are in good agreement with experimental ones at lower excitation energy but for higher excitation energy except for 14° and 17° angles, all are in good agreement. As a whole, the shapes of continuum DDX spectra, generally, are fairly well reproduced, and the absolute values of cross sections are in good agreement with and very close to the experimental data. The theoretically calculated angular distributions of analyzing powers also agree with experimental ones. These facts assure the validity of the experimental as well as the theoretical data processing method for continuum spectra.

(ii) In Fig. 12, the angular distributions of the cross sections and analyzing powers are shown as obtained after summing up over the excitation energy regions of 0–2.5, 2.5–5.8, and $0-5.8$ MeV, i.e., the peak, continuum-dominated and full region (from discrete levels to continuum spectra). The absolute value of theoretical cross section is to be multiplied by a factor of 0.75 for the $0-2.5$ MeV region to fit the experimental result; whereas, for the other two regions no such normalization is needed. For the analyzing power, it represents good agreement in magnitude. The fitting of the absolute value of theoretical cross sections to the experimental ones are in good agreement in magnitude and also in expressing the trend of angular distributions of the cross sections and analyzing powers for all the three regions except for the region dominated by the discrete levels. The last fact is natural as the model used in the analysis is not valid for a detailed structure of the ground state region. Figure 12 is also another indication for the reliability of the theoretical calculation for the shape of theoretically reproduced spectra and also for the values of cross sections which are almost similar to those of experimental ones except for peak dominated region where the normalization factor lies in the neighborhood of unity.

V. CONCLUSIONS

The ^{96}Mo$(\vec{p},d)^{95}$Mo reaction was studied with a 50 MeV polarized protons. The angular distributions of the differential cross section and analyzing power were measured for single hole states in ^{95}Mo up to an excitation energy of 5.8 MeV. The data analysis with a standard distorted wave Born approximation theory provided transferred angular momenta ℓj and spectroscopic factors of 49 excited states up to an excitation energy of $\sim$5 MeV. Two global potentials other than Becchetti and Greenlees were used here for some strong and unambiguous states to test the reliability of the C^2S values and also used in the case of continuum spectra for being confident about the theoretical method of DDX. Because of the use of polarized beam a unique assignment of spin and parity is possible for most of the levels, except a few where one or the other of the differential cross section and the analyzing power is not well fitted. Some of the previous J^π assignments, as well as ℓ transfers are contradicted in our study and a few new assignments are made; whenever an assignment is in doubt, that particular case is shown in parenthesis in Table II. One-step direct pickup reaction model was used here for analyzing the wide spectra from discrete levels to continuum region. The theoretical distribution of the strength function over the experimental continuum spectra are reproduced well by adopting an asymmetric Lorentzian form in the DWBA-based cross sections calculation having energy dependent spreading width.

ACKNOWLEDGMENTS

The authors are grateful to the staff of the Research Center for Nuclear Physics (RCNP), Osaka University, for the support of the experiments at the cyclotron facility. One of the authors (S.A.S.) acknowledges the financial support from the Ministry of Education, Science and Culture, Goverment of Japan, and the leave from Bangladesh Open University.

[1] P. G. Young, E. D. Arthur, and M. B. Chadwick, Los Alamos National Laboratory, Report No. LA-MS-12343 (1992).
[2] H. Takada, J. Nucl. Sci. Technol. **33**, 275 (1996).
[3] K. Niita, S. Chiba, T. Maruyama, T. Maruyama, H. Takada, T. Fukahori, Y. Nakahara, and A. Iwamoto, Phys. Rev. C **52**, 2620 (1995).
[4] I. Slypen, V. Corcalciuc, and J. P. Meulders, Phys. Rev. C **51**, 1303 (1995).
[5] Y. Nauchi, M. Baba, T. Sanami, M. Ibaraki, T. Iwasaki, N. Hirakawa, S. Tanaka, S. Meigo, H. Nakashima, H. Takada, T. Nakamura, and Y. Watanabe, J. Nucl. Sci. Technol. **36**, 143 (1999).
[6] M. B. Lewis, Phys. Rev. C **11**, 145 (1975).
[7] R. B. Firestone, V. S. Shirley, C. M. Baglin, S. Y. F. Chu, and J. Zipkin, *Table of Isotopes*, 8th ed. (Wiley, New York, 1996).
[8] P. K. Bindal, D. H. Youngblood, and R. L. Kozub, Phys. Rev. C **15**, 2006 (1977).
[9] S. A. Hjorth and B. L. Cohen, Phys. Rev. **135**, B920 (1964).
[10] H. Ohnuma and J. L. Yntema, Phys. Rev. **178**, 1855 (1969).
[11] R. C. Diehl, B. L. Cohen, R. A. Moyer, and L. H. Goldman, Phys. Rev. C **1**, 2132 (1970).
[12] J. Schoonover, H. C. Cheung, J. E. Kitching, S. K. Mark, and J. K. P. Lee, Z. Phys. A **272**, 99 (1975).
[13] R. C. Johnson and P. J. R. Soper, Phys. Rev. C **1**, 976 (1970).
[14] K. Hisamochi, O. Iwamoto, A. Kisanuki, S. Budihardjo, S. Widodo, A. Nohtomi, Y. Uozumi, T. Sakae, M. Matoba, M. Nakano, T. Maki, S. Matsuki, and N. Koori, Nucl. Phys. **A564**, 227 (1993).
[15] S. Hirowatari, Syafarudin, F. Aramaki, A. Nohtomi, G. Wakabayashi, Y. Uozumi, N. Ikeda, M. Matoba, Y. Aoki, K. Hirota, N. Okumura, and T. Joh, Nucl. Phys. **A714**, 3 (2003).
[16] F. Aramaki, Syafarudin, G. Wakabayashi, Y. Uozumi, N. Ikeda, M. Matoba, T. Sakae, and N. Koori, Proceedings of the 2002 Symposium on Nuclear Data, JAERI-Conf 2002-006, pp. 178–182.
[17] M. Matoba, H. Ijiri, H. Ohgaki, S. Uehara, T. Fujiki, Y. Uozumi, and H. Kugimiya, Phys. Rev. C **39**, 1658 (1989).
[18] M. Matoba, O. Iwamoto, Y. Uozumi, and T. Sakae, Phys. Rev. C **48**, 95 (1993).
[19] H. M. Sen Gupta, Syafarudin, S. Aoki, F. Aramaki, M. Matoba, Y. Uozumi, G. Wakabayashi, T. Sakae, N. Koori, T. Maki, M. Nakano, Y. Fujita, M. Fujiwara, H. Ikegami, I. Katayama, S. Morinobu, and T. Yamazaki, Phys. Rev. C **63**, 017601 (2000).
[20] M. Matoba, O. Iwamoto, Y. Uozumi, T. Sakae, N. Koori, H. Ohgaki, H. Kugimiya, H. Ijiri, T. Maki, and M. Nakano, Nucl. Phys. **A581**, 21 (1995).
[21] M. Matoba, K. Kurohmaru, O. Iwamoto, A. Nohtomi, Y. Uozumi, T. Sakae, N. Koori, H. Ohgaki, H. Ijiri, T. Maki, M. Nakano, and H. M. Sen Gupta, Phys. Rev. C **53**, 1792 (1996).
[22] M. Matoba, K. Yamaguchi, K. Kurohmaru, O. Iwamoto, S. Widodo, A. Nohtomi, Y. Uozumi, T. Sakae, N. Koori, T. Maki, and M. Nakano, Phys. Rev. C **55**, 3152 (1997).
[23] H. Ikegami, S. Morinobu, I. Katayama, M. Fujiwara, and S. Yamabe, Nucl. Instrum. Methods **175**, 335 (1980).
[24] M. Matoba, K. Tsuji, K. Marubayashi, T. Shintake, H. Ikegami, T. Yamazaki, S. Morinobu, I. Katayama, M. Fujiwara, and Y. Fujita, Nucl. Instrum. Methods **180**, 419 (1981).
[25] J. J. H. Menet, E. E. Gross, J. J. Malanify, and A. Zucker, Phys. Rev. C **4**, 1114 (1971).
[26] P. D. Kunz, DWBA code DWUCK- 4, University of Colorado (unpublished).
[27] F. D. Becchetti, Jr. and G. W. Greenlees, Phys. Rev. **182**, 1190 (1969).
[28] C. Mahaux and R. Sartor, Nucl. Phys. **A493**, 157 (1989); Adv. Nucl. Phys. **20**, 1 (1991).
[29] A. Bohr and B. R. Mottelson, *Nuclear Structure* (W. A. Benjamin, New York, 1969), Vol. 1, Appendix 2D.
[30] G. E. Brown and M. Rho, Nucl. Phys. **A372**, 397 (1981).
[31] J. B. French and M. H. Macfarlane, Nucl. Phys. **26**, 168 (1961).
[32] B. Kharraja, S. S. Ghugre, U. Garg, R. V. F. Janssens, M. P. Carpenter, B. Crowell, T. L. Khoo, T. Lauritsen, D. Nisius, W. Reviol, W. F. Mueller, L. L. Riedinger, and R. Kaczarowski, Phys. Rev. C **57**, 2903 (1998).
[33] J. M. Chatterjee, M. S. Sarkar, S. Bhattacharya, P. Banerjee, S. Sarkar, R. P. Singh, S. Murulithar, and R. K. Bhowmik, Pramana, J. Phys. **57**, 165 (2001).
[34] A. J. Koning and J. P. Delaroche, Nucl. Phys. **A713**, 231 (2003).
[35] P. K. Bindal, D. H. Youngblood, and R. L. Kozub, Phys. Rev. C **12**, 1826 (1975).
[36] J. B. Moorhead and R. A. Moyer, Phys. Rev. **184**, 1205 (1969).
[37] Y. Nedjadi and J. R. Rook, Nucl. Phys. **A585**, 641 (1995).